Hindawi
Shock and Vibration
Volume 2021, Article ID 4161545, 21 pages
https://doi.org/10.1155/2021/4161545

Research Article

Study on Vibration Response of Layered Media under the Impact Load

Mengyang Zhen[1,2,3], **Jun Liu**[1,2,3], **Zhimin Xiao**[1,2,3], **Futian Zhao**[1,2,3], **Yue Wang**[1,2,3], **Chen Ou**[1,2,3], **Zheng Liu**[1,2,3] and **Haowen Zheng**[1,2,3]

[1]*College of Civil and Transportation Engineering, Hohai University, Nanjing 210098, China*
[2]*Institute of Engineering Safety and Disaster Prevention, Hohai University, Nanjing 210098, China*
[3]*Key Laboratory of Ministry of Education for Geomechanics and Embankment Engineering, Hohai University, Nanjing 210098, China*

Correspondence should be addressed to Jun Liu; ljun8@263.net

Received 18 August 2021; Accepted 14 September 2021; Published 11 October 2021

Academic Editor: Xuepeng Zhang

To study the vibration response of the layered medium under impact loading, single-layer concrete slabs, multilayer concrete slabs, and multilayer concrete slabs with a cemented filling layer were used as the working media to simulate the layered medium. A large number of impact loading tests were carried out by using a simple drop hammer device designed by us. The experimental results indicate that, under the impact load, the vibration response of the surface of the medium decreases with the increase in the distance to the impact source, showing the law of fast attenuation near field and slow attenuation far field, and the vibration energy moves to the low-frequency component; the vibration response increases with the increase in the impact energy, and the difference in the vibration response caused by the impact energy decreases as the distance increases; the vibration response is negatively correlated with the thickness of the dielectric layer, and the divergence of vibration response caused by impact energy decreases with the increase in the thickness of the dielectric layer. Due to the existence of the free surface and bedding, the vibration response of the layered medium surface increases with the increase in the number of layers and the vibration velocity response increases with the increase in the distance to the impact source when it is close to the free surface and far from the vibration source. For the filling of the cemented layer, the vibration response of the layered concrete slab becomes more complex under impact loading, showing obvious disorder. At the same time, this paper also used the dimensional analysis method to establish the calculation model of the peak response of vibration velocity of layered media under the impact load, which provided an idea for determining the peak response of vibration velocity of the layered media.

1. Introduction

In nature and real life, layered structures and layered media widely exist in the fields of stratigraphy and geotechnical engineering. For example, most of the soil environments we face have certain delamination; the primary layered rock mass structure is represented by sedimentary rock; the plate layered rock mass structure is represented by metamorphic rock; most pavement roadbeds are designed with a minimum of three layers of media material: surface base, base layer, and bedding layer. The problem of layered media subjected to impact loads exists in all kinds of engineering and technical practice, military and protective engineering, scientific research, and other fields. Therefore, the research on the vibration response of the layered media under the impact load has always been a key research topic in the fields of civil engineering, mining engineering, civil air defense engineering, and other fields. Many scholars at home and abroad have made extensive and in-depth studies on the vibration response of layered media under impact loading from three aspects: theory, test, and numerical simulation.

The starting point for theoretical studies is the elastic dynamics, and most of the modelling methods for layered media use the transfer matrix method and the thin-layer method. Thomson [1] theoretically studied the propagation of oblique incidence of a plane elastic wave through a layered solid medium composed of any number of parallel plates with different materials and thicknesses by using the matrix method for the first time, and the functional relation is expressed in a form that is convenient for calculation. Haskell [2, 3] generalized the matrix form proposed by Thomson, calculated the phase and group velocities of Rayleigh waves in two hypothetical three-layer models of the continental crust and a two-layer model, obtained the phase velocity dispersion equations of Rayleigh and Love elastic surface waves in multilayer solid media, and extended the dispersion of Rayleigh waves caused by an arbitrary point source in an infinite homogeneous medium to a medium composed of any number of parallel uniform layers. Since the Thomson–Haskell transfer matrix method was proposed, the transfer matrix method has been successfully applied to the study of waves in multilayer media. However, there is an exponential growth term in the Thomson–Haskell matrix, which will cause numerical instability at high frequency. Pestel and Leckie [4], Knopoff [5], Thrower [6], Dunkin [7], Watson [8], Buchen and Ben-Hador [9], Chapman [10], Pei et al. [11], and Liu [12] have made many attempts to overcome the difficulties in numerical calculation at high frequency, making the numerical stability at high frequency higher as well as improving the speed of calculation at the same time. The thin-layer method is a semianalytical and half-value method to analyze and simulate wave propagation in layered soil or media. Lysmer [13] first applied the thin-layer method to analyze the propagation characteristics of Rayleigh waves in layered soils, and the group velocity and dispersion curves of surface waves were obtained. Waas [14] applied the thin-layer method to the analysis of SV-P waves and SH waves in the two-dimensional domain, achieved the transmission boundary of the two-dimensional irregular soil medium, and applied it to the famous soil-structure dynamic interaction analysis software FLUSH. By means of Fourier transform and Hankel transform, Tajimi [15], Waas et al. [16], and Kausel [17] obtained the Green function of point-source excitation in layered media by the thin-layer method, respectively, which provided the possibility for applying the thin-layer method to the boundary element method. Kausel [18] further deduced Green's function in the time domain and improved the basic solution of the thin-layer method. Sen [19] introduced the application of Green's function of the thin-layer method in the vibration of pile foundation and used Green's function obtained by the thin-layer method as semianalytical dynamic Mindlni's solution to analyze soil. Bougacha [20, 21] established the thin-layer method formulas of saturated layered media in the two-dimensional-plane, out-of-plane, and three-dimensional bedrock. Nogami and Kazmaa [22, 23] also established two-dimensional and three-dimensional thin-layer method formulas for saturated layered media, analyzed the influence of medium permeability on the dynamic response and wave propagation characteristics, and simply analyzed the vibration problem of a single pile. Sun [24] proposed a high-order thin-layer method, which improves the accuracy and stability of viscoelastic wave propagation in layered media.

Many researchers have done much work through more intuitive experimental research methods. SHPB is usually used to study wave propagation in layered media. Ju [25], Wang [26], Lu [27], and Li [28] studied the propagation characteristics of one-dimensional stress waves in layered media by fractal theory and analyzed the transmission and reflection characteristics of joints and the effects of fractal dimension and joint roughness. Similarly, based on SHPB test equipment, Li [28], Yang [29], Wei [30], and Challita [31] studied the effects of impact rate, strain rate, joint angle, joint thickness, and other parameters. In addition to the SHPB test system, Tian [32] and Sun [33] also carried out some research using the impact test equipment developed by ourselves. According to the actual blasting engineering, Li and Cheng [34] and Wang et al. [35] analyzed the wave attenuation of the natural layered foundation and improved the empirical formula of stress wave propagation.

The main numerical simulation methods of dynamic response of layered media are finite difference method (FDM), finite element method (FEM), and boundary element method (BEM). The finite difference method is efficient and easy to implement; the finite element method is capable of adapting to complex models but is more difficult to implement; the boundary element method does not involve volume discretization and can accurately deal with the geometric characteristics of the underground irregular interface.

Although many problems of vibration response of layered media can be solved by theoretical analysis and numerical simulation, in many cases, the model and boundary conditions on which the analysis is based, even the excitation of vibration, cannot fully accord with the actual situation. Especially for the vibration response of layered media with complex excitation form, complex material and structure composition, and nonhomogeneous and nonlinear problems, it is often not enough to rely solely on the existing theories and numerical calculation methods to analyze the vibration response. Therefore, the vibration test or direct vibration detection has become an important and indispensable means to analyze and study the causes and laws of vibration response. Considering that using the dimensional analysis method to analyze more complex phenomena or problems is an effective means, this paper not only carried out the experimental research on the vibration response of layered media under the impact load but also used the dimensional analysis method which fully considers the influencing factors of dynamic response of layered media. Combined with the test data of the impact test, the calculation model of the response of vibration velocity of the layered media under the impact load was built, which will provide an idea for determining the response of peak vibration velocity of the layered media.

2. Dimensional Analysis Theory

The vibration response of the layered media under the impact load is a very complex process of energy conversion and energy propagation, in which the impact of layered media and wave propagation in the layered media are completed in a very short time. At the same time, the process also involves complex transmission and reflection problems and discontinuous, nonlinear problems, which make it difficult to construct the impact dynamic response theory using existing mathematical models and mechanical principles but can be solved with the help of dimensional analysis methods.

Dimensional analysis is based on experience and experimentation, using the principle of similarity and the law of dimensional harmony to quantify each physical quantity relevant to the problem in a dimensionless way and ultimately to determine the relationship between the physical quantities. The Π theorem proposed by American physicist Buckingham [36] in 1914 is the theoretical core of dimensional analysis. The specific steps are as follows:

(1) Choose the international unit as the basic unit system and length L, mass M, and time T as the basic quantity categories, with basic units, $m \in L$, kg $\in M$, and $s \in T$.

(2) Suppose the problem involves n variables and the number $a_1, \ldots, a_n$ in the international system of units satisfies

$$f(a_1, a_2, \ldots, a_n) = 0. \tag{1}$$

Describe n variables by the dimensional formula; that is, express them as the dimensional power formula of the basic quantity

$$\dim a_i = L^{x_i} M^{y_i} T^{z_i}, \quad i = 1, 2, \ldots, n. \tag{2}$$

(3) According to the dimensional formula, establish the dimensional matrix:

$$\begin{array}{c} \\ L \\ M \\ T \end{array} \begin{array}{c} \begin{array}{cccc} a_1 & a_2 & \cdots & a_n \end{array} \\ \begin{bmatrix} x_1 & x_2 & \cdots & x_n \\ y_1 & y_2 & \cdots & y_n \\ z_1 & z_2 & \cdots & z_n \end{bmatrix} \end{array}. \tag{3}$$

(4) To rank the measured matrix, determine the group B quantities. The group B quantities can be expressed as dimensionless Π numbers from the group A quantities, and these dimensionless Π numbers form a definite functional relationship satisfying

$$g(\Pi_1, \Pi_2, \ldots \Pi_{n-k}) = 0. \tag{4}$$

3. Experimental Preparations

Vibration test is an effective method to study shock vibration characteristics and propagation laws, and the test data can be used for the study of shock vibration response. In this paper, a self-developed simple drop hammer impact loading device was used to conduct experimental research on impact vibration testing of layered media.

3.1. Drop Hammer Impact Loading Device. Explosive, falling weight and hammering are commonly used in practical applications to carry out research work under impact loading. In this research, for the sake of simplicity, a simple drop-weight impact loading device was designed by us. The device consists of a drop-weight lifting device and a drop-weight device. The drop hammer lifting device includes two steel pipes with bases, two movable support frames sleeved on the steel pipes, a connecting rod, and a fixed pulley lapped on the support frame, as shown in Figure 1. The maximum drop height of the drop hammer can be controlled by adjusting the movable support frame up to a maximum drop height of 1.2 m. The hammer is connected to a tow rope at the end of the hammer to form the hammer drop device, which weighs 2.5 kg, as shown in Figure 2, and the specific parameters of the hammer are shown in Table 1. Manual control of the haul rope enables the hammer to fall freely and to regulate the drop height, which controls the impact energy/force by adjusting the drop height.

3.2. Test Instrument. The test instrument is the MinimatePro4TM vibration and overvoltage monitor produced by the Canadian company Instantel, which is connected to an ISEE standard or DIN standard three-way detector. The test instrument is shown in Figure 3. It provides 64 megabytes of storage, and the vibration monitoring range is 0.13~25 mm/s. The test parameter is the vibration velocity. The vibration velocity trigger value is set to 5.0 mm/s, the sampling frequency is 2048 samples/s, the sampling time is 3.0 s, and the sampling mode is automatic sampling.

3.3. Specimen Processing. Concrete materials are widely used in civil engineering due to their stable mechanical properties and the ease of adjusting their proportions. Therefore, the concrete material was selected as the test object in this experiment. The design concrete strength grade was C25, and the concrete ratio was water: cement: sand: stone = 0.38 : 1 : 1.11 : 2.72. We used P.O42.5 ordinary Portland cement and melon seed flake stones with a particle size of less than 20 mm as raw materials. The length and width of the concrete slab was determined as 2.5 m × 1 m. The thicknesses were, respectively, 5 cm, 10 cm, 15 cm, and 20 cm. Due to the large size of the concrete slab, to prevent the concrete slab from breaking during the subsequent lifting process, steel bars were embedded in the concrete slab. The model size and reinforcement of the concrete slab are shown in Table 2.

The mold should be made in advance before the concrete slab is poured, and a layer of the release agent should be applied to the inside of the mold. The reinforcement is then designed, processed, and configured. The mixed concrete is then added to the mold and vibrated in layers with a vibrating bar. Once the concrete surface appears floating, it can be smoothed out with a clay trowel (Figure 4).

Figure 1: Drop hammer lifting device.

Figure 2: Physical map of the hammer.

Table 1: Specific parameters of the hammer.

Mass of the drop hammer m (kg)	Elastic modulus E (GPa)	Density ρ (kg/m^3)
2.5	200	8300

Figure 3: Vibration and overvoltage monitor MinimatePro4TM.

Table 2: Model size and reinforcement of the concrete slab.

Model	Size (cm × cm × cm)	Reinforcement	Quantity (n)
B1	250 × 100 × 5	Ø6@100	4
B2	250 × 100 × 10	Ø6@125	4
B3	250 × 100 × 15	Ø6@150	1
B4	250 × 100 × 20	Ø6@150	1

To determine the actual strength of concrete, five standard cube blocks of 150 mm × 150 mm × 150 mm were made by mixing concrete at the same time of pouring concrete slabs. After the specimen had been released, the standard test block and the cast model were cured under the same conditions for 28 days. The compressive strength of the concrete was measured at 23.64 MPa by compression testing of standard specimens on an intelligent force measuring instrument, type RFP-03, at the end of the maintenance stage.

3.4. Materials of the Cemented Filling Layer. In nature and practical engineering, the interface of layered media is usually accompanied by weak thin interlayers, such as cemented soft rock, cemented muddy material, and cemented sand-gravel thin layer in layered geotechnical media. One of the basic purposes of the test was to analyze the effect of the material and thickness of the cemented thin sandwich on the vibration response of the layered medium. Based on this consideration, three materials with different moduli of elasticity were used to simulate the infill binder, namely, EPE pearl cotton, XPS extruded board, and sand, as shown in Figure 5. These three kinds of materials all have good fit. Three different materials were placed between the concrete slabs as a cemented filling layer, and the drop hammer impact loading test was carried out. The relevant parameters of the cemented layer material are shown in Tables 3–5.

4. Experimental Process

4.1. Operating Conditions. The self-designed simple drop hammer impact loading device was used to carry out the impact test of the concrete slab. During the test, the impact energy was controlled by changing the drop height of the hammer. To study the influence of layer thickness, layer number, cemented layer material, and thickness on the impact performance of layered media, the combinations of concrete slabs were divided into three types: (1) single-layer concrete slabs; (2) multilayer concrete slabs without cemented filling layer; (3) multilayer concrete slabs containing a cemented filling layer. The drop-weight impact loading test of the single-layer concrete slab includes 24 test conditions with 4 different concrete slab thicknesses and 6 drop heights. Three repeated tests were carried out for each working condition, and a total of 72 tests were carried out. The test conditions are shown in Table 6. The drop-weight impact loading test of multilayer concrete slabs without the cemented filling layer includes 24 test conditions with different layers and drop heights. Three repeated tests were carried out for each working condition, and a total of 72 tests were carried out. The test working conditions are shown in Table 7. The drop-weight impact loading test of multilayer concrete slabs with cemented filling layers includes 30 test conditions of different cemented layer materials, thicknesses, and drop heights. Three repeated tests were carried out for each working condition, and 90 tests were carried out in total. The test working conditions are shown in Table 8.

4.2. Test Procedure. The specific operation steps of the drop-weight impact loading test are as follows: (1) we selected a leveling site, used the crane to put the concrete slabs to the designated position of the site, and arranged them in a combined form; (2) we used a plaster with good coupling to fix the sensor on the designated position as the measuring point; (3) we manually controlled the traction rope to adjust the drop height of the hammer to make it fall freely and impact the concrete slab; (4) we recorded the impact response of each measuring point; (5) the test was repeated three times under the same condition to eliminate the influence of accidental errors on the test results during the test process.

4.3. Layout of Measuring Points. There were 7 measuring points arranged on the surface of the uppermost concrete slab: P1~P7. The seven measuring points were arranged parallel to the long edge of the concrete slab along the surface centerline of the concrete slab, and the relationship between the measuring points and the bedding trend was parallel. The distances from P1~P7 to the impact point were 0.3 m, 0.6 m, 0.9 m, 1.2 m, 1.5 m, 1.8 m, and 2.1 m, respectively. The specific arrangement of measuring points is shown in Figure 6. The vibration response of each measuring point is recorded after the impact loading of the drop hammer device. The layout of the measuring points on the test site is shown in Figure 7.

5. Experimental Results and Discussion

Vibration velocity is an important indicator reflecting the impact response characteristics of the measuring point. The magnitude of the impact response and the dynamic mechanical properties of the impacted object can be reflected from the vibration velocity. The MinimatePro4TM vibration and overpressure monitor allows the measurement of vibration velocities in the vertical and horizontal (longitudinal and transverse) directions at the measuring point, the physical quantities evaluated in most studies being mainly the vertical vibration response. Therefore, in this paper, the peak particle velocity (PPV) was selected as the index to analyze the vibration test data. Under the same test conditions, each impact loading had certain randomness; in order to reduce the influence of chance errors on the experimental results, each group of tests were repeated three times. In the data processing of the peak vertical vibration velocity, the test data with large dispersions were excluded and the mean value was obtained.

Figure 4: Concrete slab processing.

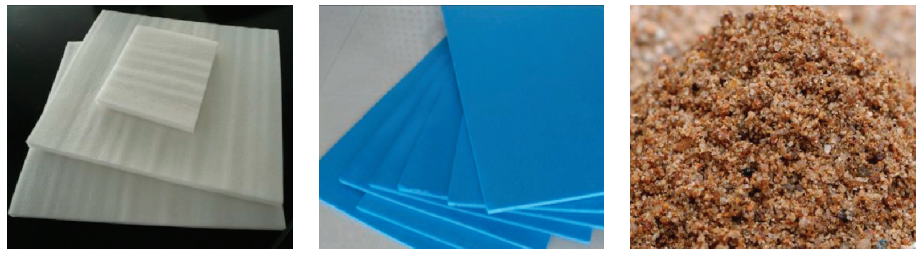

(a) (b) (c)

Figure 5: Material of the cemented filling layer. (a) EPE pearl cotton. (b) XPS extruded board. (c) Sand.

Table 3: EPE pearl cotton parameters.

Density	Yield strength (kPa)	Elastic modulus (MPa)	Poisson's ratio	Hardening constant
20.408 kg/m^3	10.18	1.6	0.4	0.342

Table 4: XPS extruded board parameters.

Density	Compressive strength (kPa)	Elastic modulus (MPa)	Poisson's ratio	Thermal conductivity
31.429 kg/m^3	150	8.5	0.345	0.26 W/m

Table 5: Sand parameters.

Density	Cohesion (kPa)	Elastic modulus (MPa)	Void ratio	Internal friction angle (°)
2056.122 kg/m^3	5.67	20.35	0.564	35.19

Table 6: Working conditions of the drop hammer impact loading test of single-layer concrete slabs.

Serial number	Plate thickness (h/cm)	Falling height (H/m)	Frequency
1	5	0.2	3
2	5	0.4	3
3	5	0.6	3
4	5	0.8	3
5	5	1.0	3
6	5	1.2	3
7	10	0.2	3
8	10	0.4	3
9	10	0.6	3
10	10	0.8	3
11	10	1.0	3
12	10	1.2	3
13	15	0.2	3
14	15	0.4	3
15	15	0.6	3

Table 6: Continued.

Serial number	Plate thickness (h/cm)	Falling height (H/m)	Frequency
16	15	0.8	3
17	15	1.0	3
18	15	1.2	3
19	20	0.2	3
20	20	0.4	3
21	20	0.6	3
22	20	0.8	3
23	20	1.0	3
24	20	1.2	3

Table 7: Working conditions of the drop-weight impact loading test of multilayer concrete slabs without the cemented filling layer.

Serial number	Combination form of the concrete slab (h/cm)	Falling height (H/m)	Frequency
1	5 cm × 2	0.2	3
2	5 cm × 2	0.4	3
3	5 cm × 2	0.6	3
4	5 cm × 2	0.8	3
5	5 cm × 2	1.0	3
6	5 cm × 2	1.2	3
7	5 cm × 3	0.2	3
8	5 cm × 3	0.4	3
9	5 cm × 3	0.6	3
10	5 cm × 3	0.8	3
11	5 cm × 3	1.0	3
12	5 cm × 3	1.2	3
13	5 cm × 4	0.2	3
14	5 cm × 4	0.4	3
15	5 cm × 4	0.6	3
16	5 cm × 4	0.8	3
17	5 cm × 4	1.0	3
18	5 cm × 4	1.2	3
19	10 cm × 2	0.2	3
20	10 cm × 2	0.4	3
21	10 cm × 2	0.6	3
22	10 cm × 2	0.8	3
23	10 cm × 2	1.0	3
24	10 cm × 2	1.2	3

Table 8: Working conditions of the drop-weight impact loading test of multilayer concrete slabs without the cemented filling layer.

Serial number	Combination form of the concrete slab (h/cm)	Falling height (H/m)	Frequency
1	10 cm × 2 + 1 cm cemented layer of the extruded board	0.8	3
2	10 cm × 2 + 1 cm cemented layer of the extruded board	1.0	3
3	10 cm × 2 + 1 cm cemented layer of the extruded board	1.2	3
4	10 cm × 2 + 1 cm cemented layer of pearl cotton	0.8	3
5	10 cm × 2 + 1 cm cemented layer of pearl cotton	1.0	3
6	10 cm × 2 + 1 cm cemented layer of pearl cotton	1.2	3
7	10 cm × 2 + 1 cm cemented layer of sand	0.8	3
8	10 cm × 2 + 1 cm cemented layer of sand	1.0	3
9	10 cm × 2 + 1 cm cemented layer of sand	1.2	3
10	10 cm × 3 + 1 cm × 2 cemented layer of the extruded board	0.8	3
11	10 cm × 3 + 1 cm × 2 cemented layer of the extruded board	1.0	3
12	10 cm × 3 + 1 cm × 2 cemented layer of the extruded board	1.2	3
13	10 cm × 3 + 1 cm × 2 cemented layer of pearl cotton	0.8	3
14	10 cm × 3 + 1 cm × 2 cemented layer of pearl cotton	1.0	3
15	10 cm × 3 + 1 cm × 2 cemented layer of pearl cotton	1.2	3
16	10 cm × 3 + 1 cm × 2 cemented layer of sand	0.8	3
17	10 cm × 3 + 1 cm × 2 cemented layer of sand	1.0	3
18	10 cm × 3 + 1 cm × 2 cemented layer of sand	1.2	3

Table 8: Continued.

Serial number	Combination form of the concrete slab (h/cm)	Falling height (H/m)	Frequency
19	10 cm × 2 + 2 cm cemented layer of the extruded board	0.8	3
20	10 cm × 2 + 2 cm cemented layer of the extruded board	1.0	3
21	10 cm × 2 + 2 cm cemented layer of the extruded board	1.2	3
22	10 cm × 2 + 3 cm cemented layer of the extruded board	0.8	3
23	10 cm × 2 + 3 cm cemented layer of the extruded board	1.0	3
24	10 cm × 2 + 3 cm cemented layer of the extruded board	1.2	3
25	10 cm × 3 + 2 cm × 2 cemented layer of the extruded board	0.8	3
26	10 cm × 3 + 2 cm × 2 cemented layer of the extruded board	1.0	3
27	10 cm × 3 + 2 cm × 2 cemented layer of the extruded board	1.2	3
28	10 cm × 3 + 3 cm × 2 cemented layer of the extruded board	0.8	3
29	10 cm × 3 + 3 cm × 2 cemented layer of the extruded board	1.0	3
30	10 cm × 3 + 3 cm × 2 cemented layer of the extruded board	1.2	3

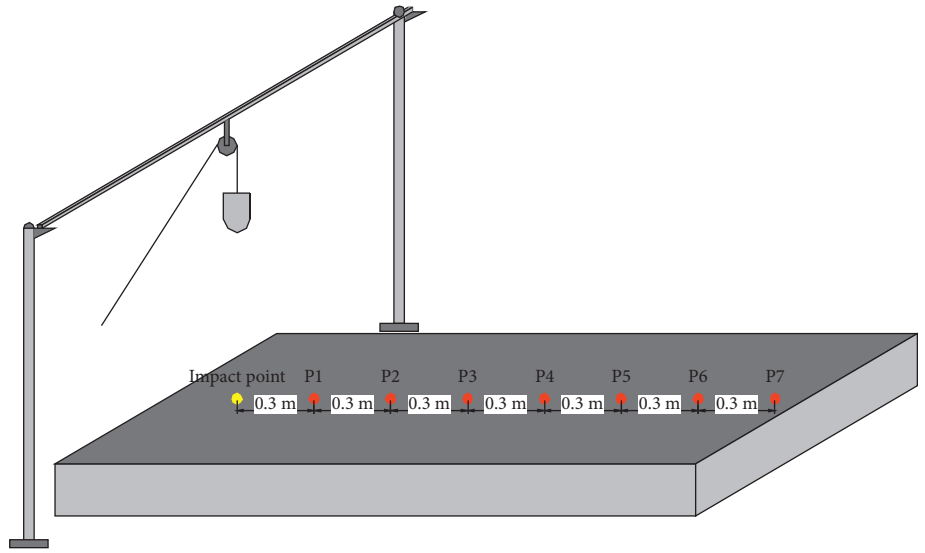

Figure 6: Schematic diagram of the measuring point layout.

Figure 7: Layout of onsite measuring points.

5.1. Impact Loading Test Results and Discussion of Single-Layer Concrete Slabs

5.1.1. Time-Frequency Analysis of Vibration Velocity. During the test, the impact loading of the single-layer concrete slab under different energies was realized by controlling the drop height. The vibration response characteristics of the medium under the impact load and the effect of impact energy, distance, and layer thickness on the vibration response were studied.

Figure 8 shows a typical vibration waveform after the completion of drop hammer impact loading. The analysis shows that the collision between the hammer and the concrete slab is somewhere between an elastic and a completely inelastic collision. After the impact of the hammer on the concrete slab, a rebound occurred, resulting in a "multiple impact" phenomenon. As can be seen from the figure, the subsequent "rebound waveforms" do not interfere with the first wave. Therefore, the influence of the phenomenon of "multiple shocks" on the vibration test after shock loading can be ignored, and only the first wave including the peak value of vibration velocity can be analyzed and studied.

To study the vibration response characteristics of the medium caused by the impact load, the frequency-domain signal of the vibration response under the impact loading is obtained through the fast Fourier transform of the measured time-domain signal and then the time-frequency characteristics of the medium vibration caused by the impact load

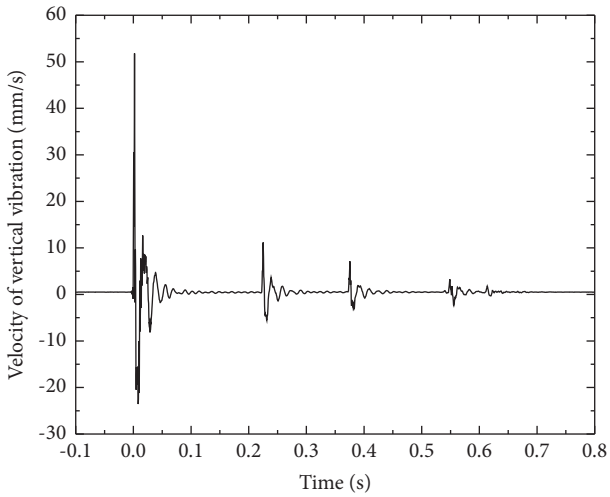

Figure 8: Typical vibration waveform.

are analyzed. Taking the working condition of a 15 cm-thick single-layer concrete slab at a drop height of 0.8 m as an example, Figures 9 and 10, respectively, show the vertical vibration waveform and frequency spectrum of each measuring point.

From the vibration waveforms of the measuring points, it can be found that the vibration response of the impact load is characterised by a short duration, with a large change in magnitude in a very short period of time and a rapid peak, followed by a fluctuating decline. A comparison of the vibration waveforms at each measuring point shows that there is a strong relationship between the vibration response of the measuring point and the distance. With the increase in distance, the amplitude of vibration velocity attenuates with distance due to the diffusion of energy and the damping of materials in the process of vibration propagation. When the vibration propagates to the vicinity of the measuring point 5 and continues to propagate far away, the vibration is superimposed due to the transmission and reflection of the free surface of the boundary and the amplitude of the vibration velocity increases with distance. It can also be seen that as the distance increases, because some high-frequency components are filtered out, the vibration waveform gradually becomes smoother and the vibration period becomes longer.

From the frequency-spectrum curve of the measuring point, it can be found the vibration caused by the falling hammer impact on the concrete slab belongs to the wide-frequency vibration, with a frequency range of 0~1024 Hz. At the distance of 0.3 m from the impact source, the main components of the vibration frequency are concentrated in the 50~240 Hz and 525~600 Hz bands. With the increase in the distance, the range and spectral values of the main components of the vibration frequency gradually decrease. At the distance of 1.2 m from the impact source, the main components of the frequency are concentrated in 50~150 Hz. As the distance continues to increase, the amplitude increases and some new high-frequency components are generated, with the main components of the frequency

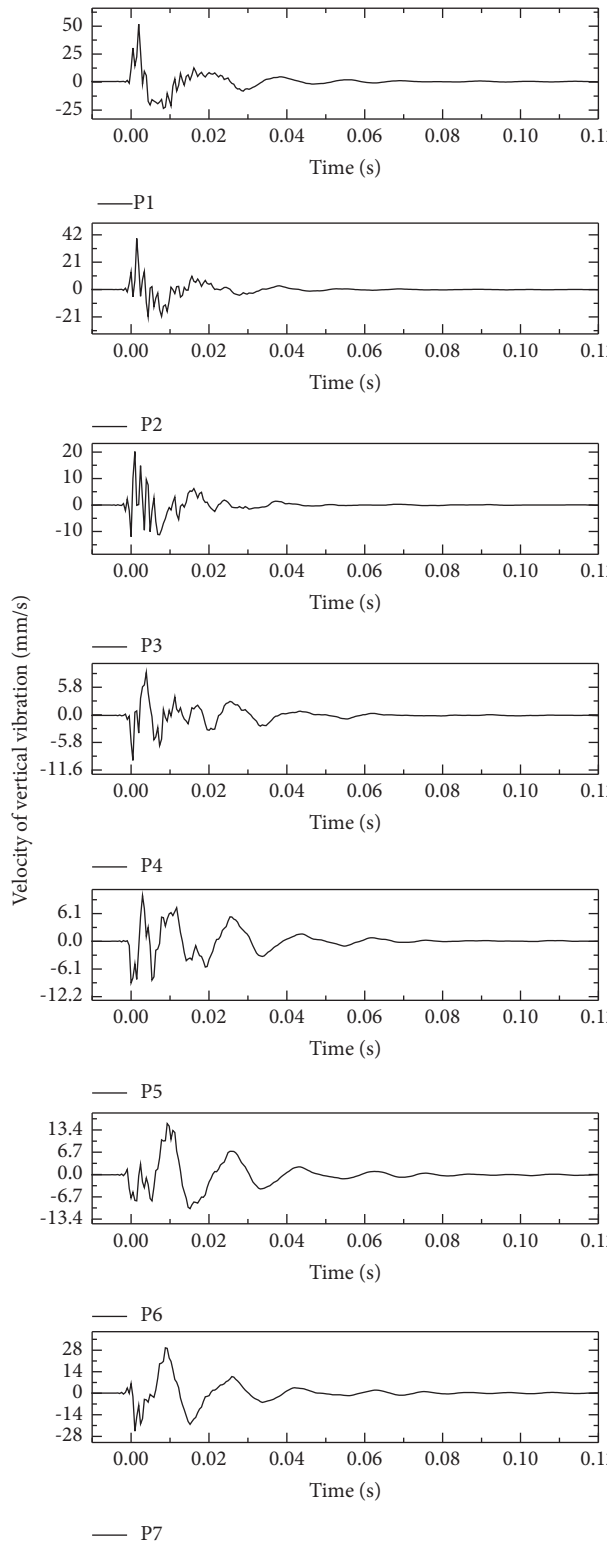

Figure 9: Vertical vibration waveforms of each measuring point.

concentrated in the 50–100 Hz range at 2.1 m from the impact source. It can be seen that the vibration energy moves to the low-frequency component with the increase in distance. This is because the high-frequency vibrations have a large number of vibrations per unit time and are subjected to

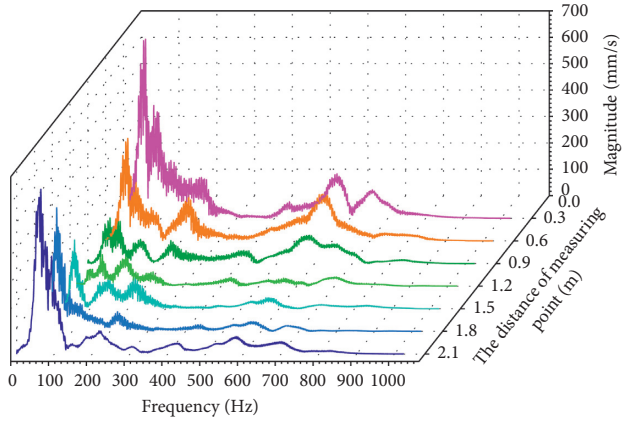

Figure 10: Vertical vibration spectrum of each measuring point.

a large damping effect, resulting in a faster decay rate. When the vibration propagates to the free surface near the side away from the source, the presence of the free surface causes the vibration wave to produce a series of transmissions and reflections and the superposition of these waves makes the amplitude increase and the frequency become higher.

5.1.2. Analysis of the Peak Value of Vibration Velocity. Taking the peak particle velocity (PPV) response as an index for the analysis, the test results for each condition were obtained by eliminating the more discrete test data from the three sets of parallel tests and finding the mean value. Under the conditions of 4 thicknesses of 5 cm, 10 cm, 15 cm, and 20 cm, Figure 11 shows the peak values of the vertical vibration velocity of each measuring point when the falling height changes.

It can be seen from the Figure 11 that the peak vibration velocity at measuring point 7 increases to varying degrees compared to measuring point 6 for different plate thicknesses and the increase becomes greater as the thickness increases. This is due to the reflection effect of the boundary-free surface, which causes the incident and reflected waves to be superimposed to a certain extent near measuring point 7, resulting in an increase in the velocity response of the mass near the free surface.

Under the impact load, the peak values of vertical vibration velocity of points 1–6 decrease with the increase in the distance from the measuring point to the impact point. And, it shows the law that the near-field attenuation is fast and the far-field attenuation is slow and tends to be smooth. Take the case of a 5 cm-thick concrete slab with a height of 1.0 m as an example. In the case of a 5 cm-thick concrete slab with a drop height of 1.0 m, the peak vertical vibration velocity measured at point 4, 1.5 m away from the impact point, decreases to 41.18% of that measured at point 1, 0.3 m away from the impact point. The peak vertical velocity measured at point 6, 1.8 m away from the impact point, decreases to 31.01% of point 1, 0.3 m away from the impact point. This is because the near-field vibration is dominated by the body wave component, which decays quickly, and the far-field vibration, where the vibration component is dominated by the surface wave, which decays slowly.

The higher the drop height, the greater the impact energy and the greater the vibration response caused by the impact of the falling hammer, given a certain thickness. The discrepancy of vibration velocity response due to impact energy decreases with increasing distance. This is because as the distance increases, the vibration energy mainly moves to the lower-frequency component, which decays slowly in the medium.

In order to analyze the effect of thickness on the response to vibration velocity, the peak vertical vibration velocity responses at point 4, 1.5 m away from the impact point, were compared for different layer thicknesses, as shown in Figure 12.

It can be seen from Figure 12 that, for the same drop height and the same test distance, the peak velocity response at the measuring point decreases as the media layer thickness increases. And, as the thickness of the medium increases, the difference in the peak response of the vibration velocity caused by the impact energy gradually decreases.

5.1.3. Dimensional Analysis. There are many factors affecting the vibration response of the medium under impact loading. For single-layer concrete slabs, they mainly include drop-weight mass m, drop height H, gravity acceleration g, drop-weight density ρ_1, elastic modulus of hammer E_1, thickness of concrete slab h, density of concrete slab ρ_2, elastic modulus of concrete slab E_2, and distance from the measuring point to impact point R. We have the following cases:

(1) According to the main influencing factors, the objective function of the peak vertical velocity is determined to be

$$f\left(\rho_1, E_1, R, m, g, H, \rho_2, E_2, h, v\right) = 0. \quad (5)$$

(2) Using the international unit system, L, M, and T (length, mass, and time) are selected as the basic dimensions, the vibration velocity and these main influencing factors are dimensionless, and the dimensional formulas expressed in the power form of the basic dimension are $\dim v = L^1M^0T^{-1}$, $\dim \rho_1$

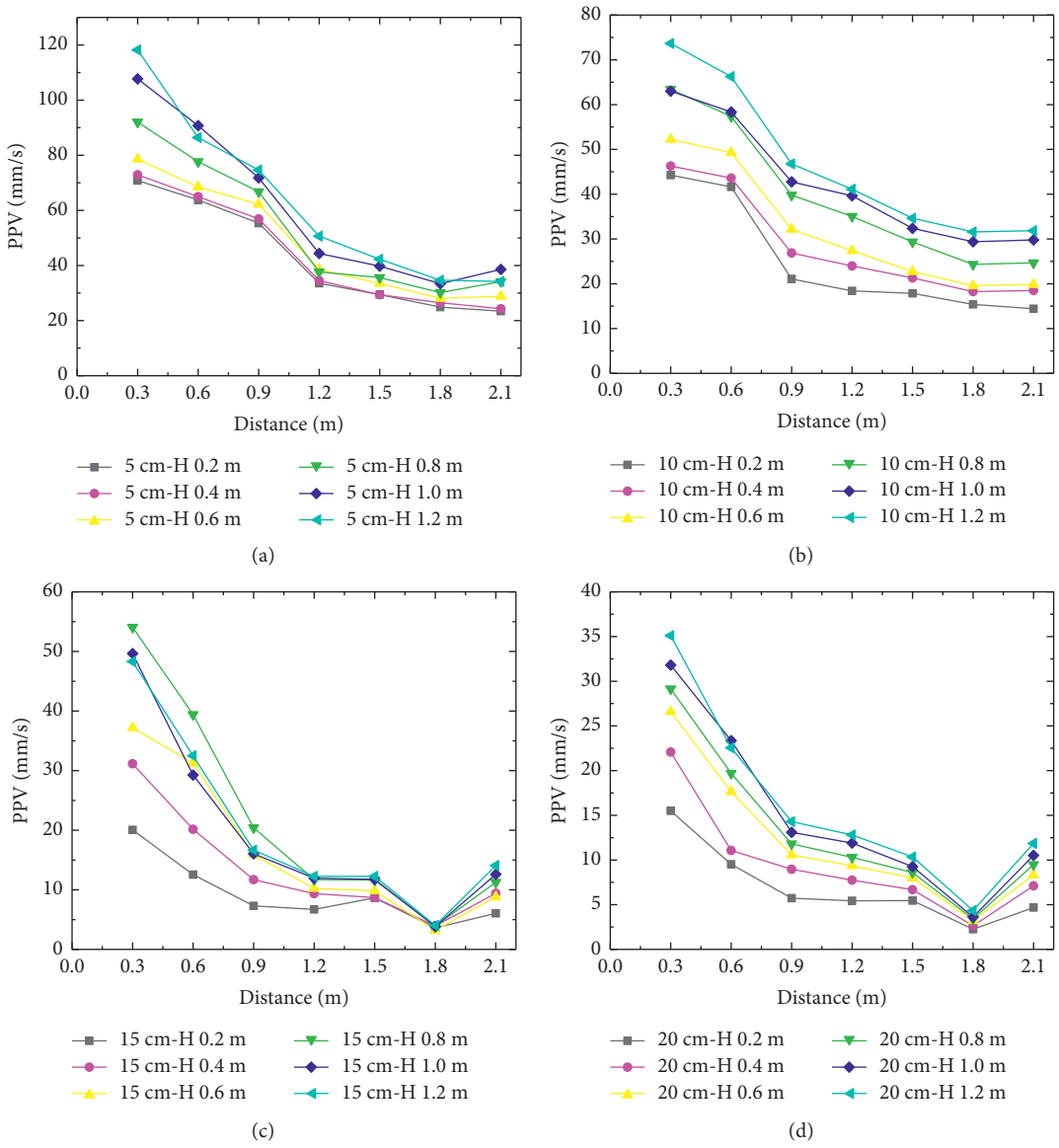

Figure 11: Peak vertical velocity of single-layer concrete slabs with different thicknesses: (a) 5 cm; (b) 10 cm; (c) 15 cm; (d) 20 cm.

$= L^{-3}M^{1}T^{0}$, $\dim E_1 = L^{-1}M^{1}T^{-2}$, $\dim m = L^{0}M^{1}T^{0}$, $\dim g = L^{1}M^{0}T^{-2}$, $\dim H = L^{1}M^{0}T^{0}$, $\dim h = L^{1}M^{0}T^{0}$, $\dim \rho_2 = L^{-3}M^{1}T^{0}$, $\dim E_2 = L^{-1}M^{1}T^{-2}$, and $\dim R = L^{1}M^{0}T^{0}$.

(3) According to the dimensional formula of each quantity, the dimensional matrix is established:

$$\begin{array}{c} \\ L \\ M \\ T \end{array} \begin{array}{c} \begin{array}{cccccccccc} \rho_1 & E_1 & R & m & g & H & \rho_2 & E_2 & h & \nu \end{array} \\ \begin{bmatrix} -3 & -1 & 1 & 0 & 1 & 1 & -3 & -1 & 1 & 1 \\ 1 & 1 & 0 & 1 & 0 & 0 & 1 & 1 & 0 & 0 \\ 0 & -2 & 0 & 0 & -2 & 0 & 0 & -2 & 0 & -1 \end{bmatrix} \end{array}. \tag{6}$$

(4) The rank of the dimensional matrix is calculated, and the rank $r = 3$ of the matrix is obtained. As a result, the number of group A is determined to be 3 and ρ_1, E_1, and R are determined as the quantity of group A. The number of group B is 10–3 = 7. The dimensionless Π number corresponding to seven group B quantities is composed of group A quantities. The specific calculation steps are as follows:

$$\dim m = (\dim \rho_1)^{x_1} (\dim E_1)^{x_2} (\dim R)^{x_3},$$

$$L^{0}M^{1}T^{0} = \left(L^{-3}M^{1}T^{0}\right)^{x_1} \left(L^{-1}M^{1}T^{-2}\right)^{x_2} \left(L^{1}M^{0}T^{0}\right)^{x_3},$$

$$\begin{cases} -3x_1 - x_2 + x_3 = 0, \\ x_1 + x_2 = 1, \\ -2x_2 = 0, \end{cases} \Rightarrow \begin{cases} x_1 = 1, \\ x_2 = 0, \\ x_3 = 3, \end{cases}$$

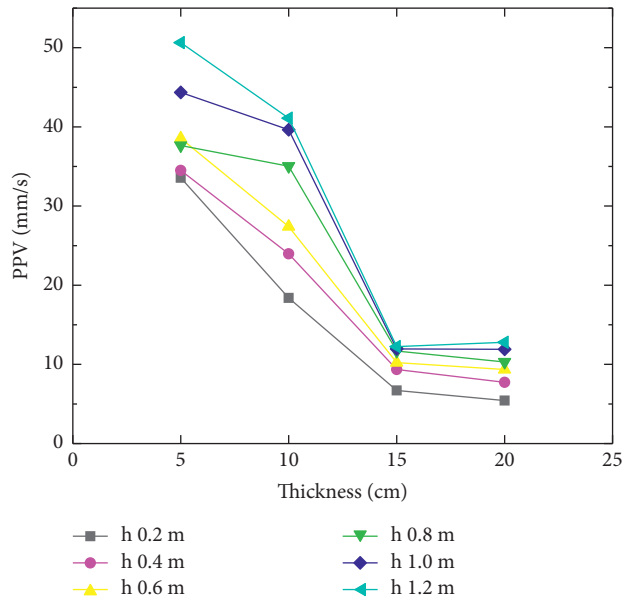

Figure 12: Comparison of peak response of vertical vibration velocity of single-layer concrete slabs with different thicknesses.

$$\dim m = (\dim \rho_1)^1 (\dim E_1)^0 (\dim R)^3,$$
$$\Pi_1 = \frac{m}{\rho_1 R^3}. \tag{7}$$

In the same way, $\Pi_2 = (g\rho_1 R/E_1)$, $\Pi_3 = (H/R)$, $\Pi_4 = (\rho_2/\rho_1)$, $\Pi_5 = (E_2/E_1)$, $\Pi_6 = (h/R)$, and $\Pi_7 = v\sqrt{(\rho_1/E_1)}$.

(5) As a result, the equivalent relation of the objective function can be obtained, and the function relation is established as follows:

$$g\left(\frac{m}{\rho_1 R^3}, \frac{g\rho_1 R}{E_1}, \frac{H}{R}, \frac{\rho_2}{\rho_1}, \frac{E_2}{E_1}, \frac{h}{R}, v\sqrt{\frac{\rho_1}{E_1}}\right) = 0. \tag{8}$$

Also, we have

$$v\sqrt{\frac{\rho_1}{E_1}} = \phi\left(\frac{m}{\rho_1 R^3}, \frac{g\rho_1 R}{E_1}, \frac{H}{R}, \frac{\rho_2}{\rho_1}, \frac{E_2}{E_1}, \frac{h}{R}\right). \tag{9}$$

Under the test conditions, the design strength, pouring environment, maintenance conditions, and cycle of the concrete slab are the same, which has little influence on the research content. The influence of weakly correlated Π number can be ignored during the calculation. Formula (9) can be simplified to

$$v\sqrt{\frac{\rho_1}{E_1}} = \phi\left(\frac{m}{\rho_1 R^3}, \frac{g\rho_1 R}{E_1}, \frac{H}{R}, \frac{h}{R}\right). \tag{10}$$

Based on the experimentally measured data and the hammer parameters, the multivariate linear function and multivariate power function are used to analyze the dimensionless Π numbers in the formula. Due to the size effect of the test object and the free surface of the boundary, the vibration response at measuring point 7 showed an increase in bounce. Therefore, point 7 was excluded from the data sample selection. The functional relationship of the peak vertical vibration velocity of the single-layer concrete slab under impact loading is obtained as follows:

(1) Multiple linear regression is

$$v = 0.075 + 2.8716\frac{m}{\rho_1 R^3} - 76159\frac{g\rho_1 R}{E_1} + 0.0116\frac{H}{R} - 0.0.1701\frac{h}{R}. \tag{11}$$

Goodness of fit of the regression model is $R^2 = 0.8391$.

(2) Multiple power function regression is

$$v = \left(\frac{m}{\rho_1 R^3}\right)^{0.6039}\left(\frac{g\rho_1 R}{E_1}\right)^{0.1041}\left(\frac{H}{R}\right)^{0.3496}\left(\frac{h}{R}\right)^{-1.2263}. \tag{12}$$

Goodness of fit of the regression model is $R^2 = 0.8664$.

By comparing the goodness of fit of the two sets of functions obtained by regression analysis, it is determined that the peak vertical vibration velocity function in the form of multivariate power function is more reasonable. Figure 13 shows the error between the fitted and experimental values after the power function regression. The residual sum of squares after regression with the power function is $RSS = 0.0287747$, and the root mean square error is RMSE = 0.014136.

5.2. Impact Loading Test Results and Discussion of Multilayer Concrete Slabs without a Cemented Filling Layer

5.2.1. Analysis of the Peak Value of Vibration Velocity. In relation to single-layer media, layered media have a layered, discontinuous character. Therefore, it is more difficult to study the dynamic mechanical response mechanism of the layered media under impact loading. Specifically, wave propagation in the layered media is complicated by the reflection and transmission effects of the laminae and boundary-free surfaces. Related studies have shown that the propagation and attenuation of stress waves in the layered media are closely related to the material properties and bedding and boundary conditions of each layer, which reflects the coupling effect of the medium, bedding, and boundary.

The concrete slabs were stacked together using a crane to simulate the layered medium. The total thickness was controlled to remain constant, and the number of layers of the concrete slab was varied to carry out impact loading tests on multilayer concrete slabs without a cemented infill layer. The influence of the number of medium layers on the dynamic response of the layered media under impact loading was studied.

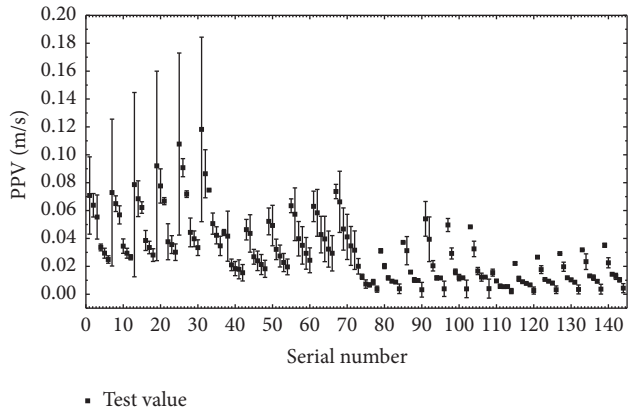

Figure 13: Error between the fitted and experimental values.

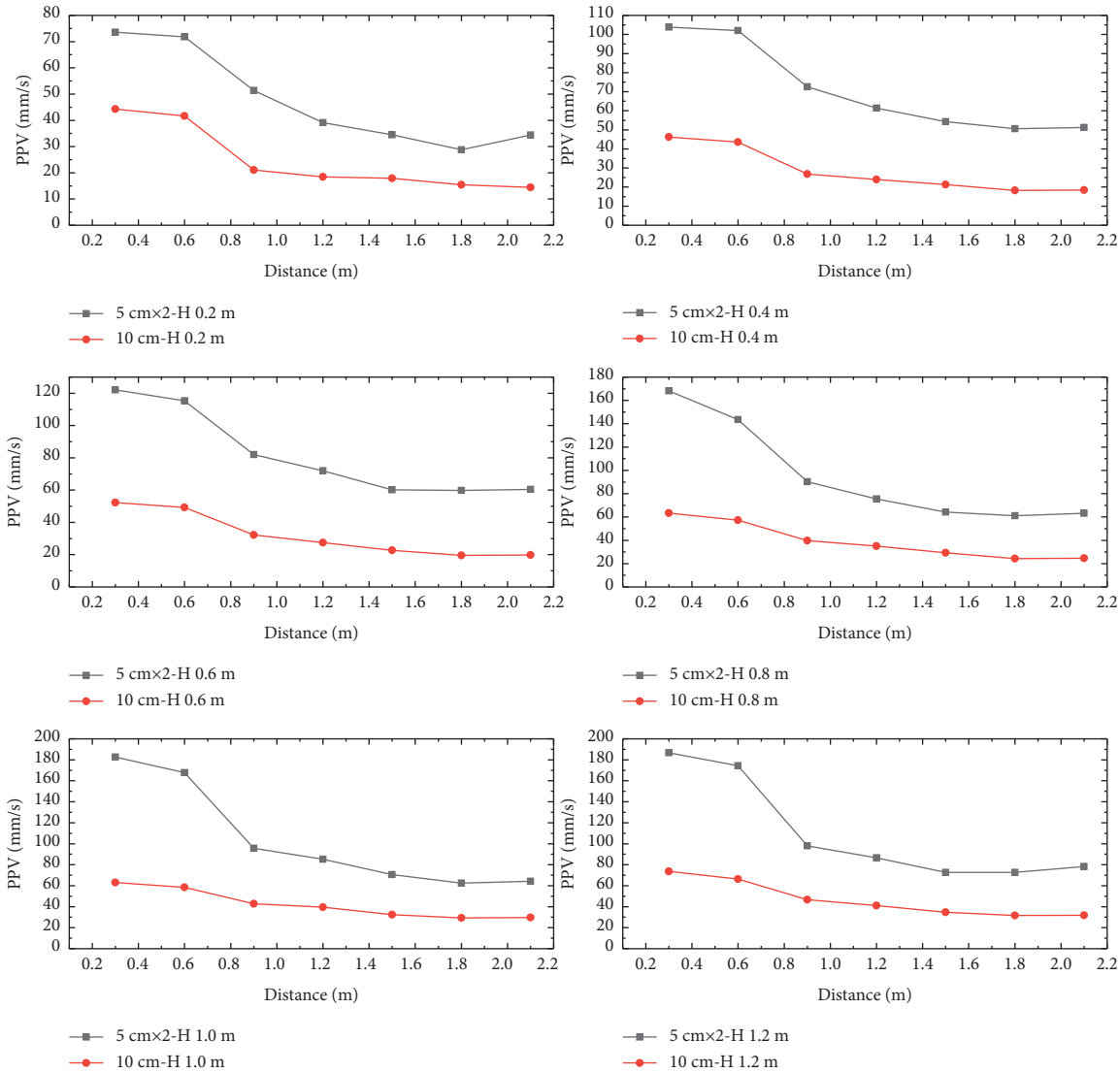

Figure 14: Peak vertical vibration velocity of multilayer concrete slabs without a cemented filling layer: 5 cm × 2 and 10 cm.

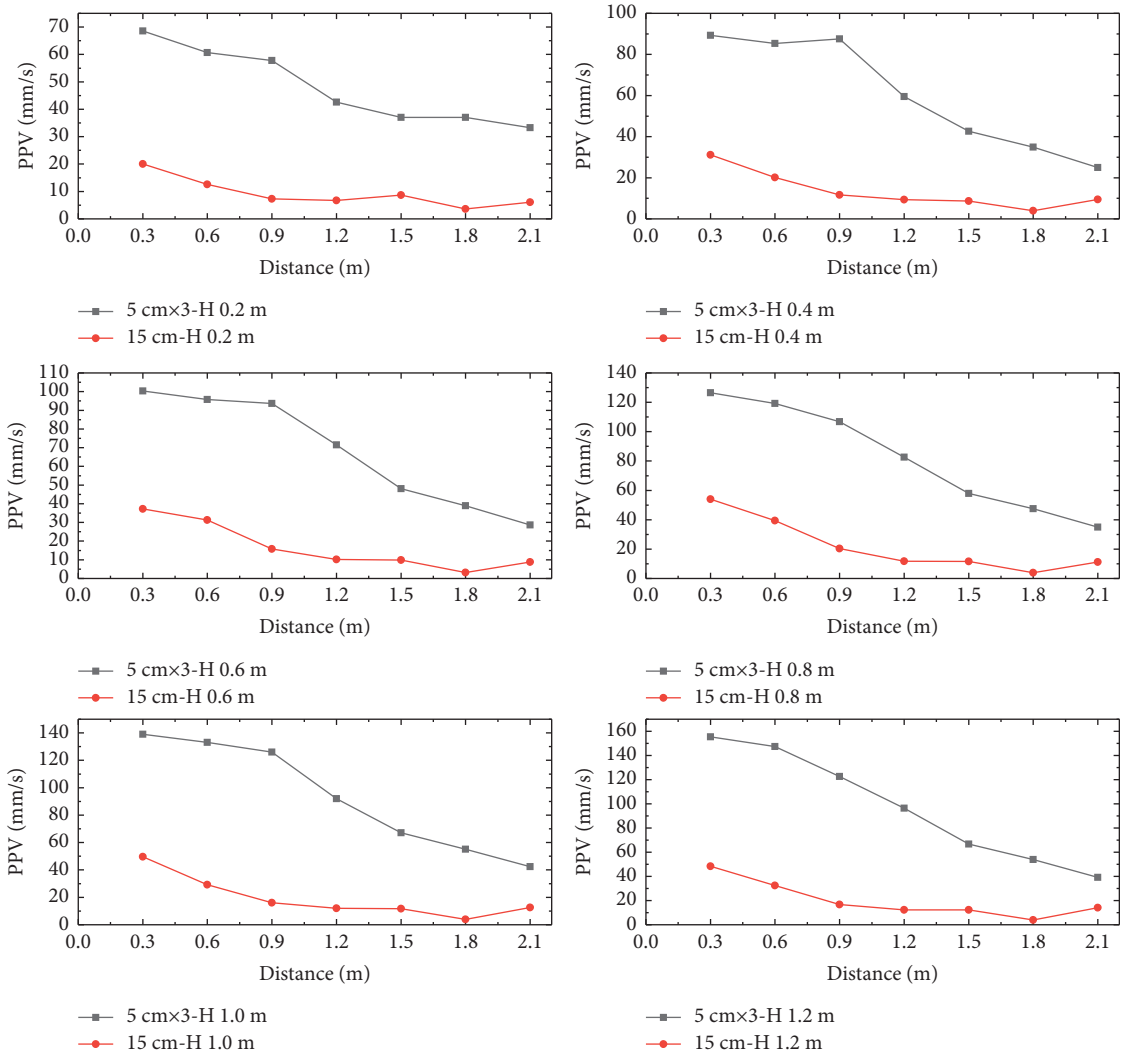

Figure 15: Peak vertical vibration velocity of multilayer concrete slabs without a cemented filling layer: 5 cm × 3 and 15 cm.

After impact loading with the simple drop hammer device, the results were compared for 5 cm × 2 and 10 cm-thick concrete slabs, 5 cm×3 and 15 cm-thick concrete slabs, and 5 cm × 4 and 10 cm × 2 and 20 cm-thick concrete slabs.

As can be seen in Figures 14–16 , the vibration response of a multilayer concrete slab without a cemented infill layer is similar to that of single-layer concrete slabs. Under the impact load, with the increase in the distance to the impact point, the peak vertical vibration velocity of the layered concrete slabs shows a decreasing trend and shows the law of fast decay in the near field and slow decay in the far field. The existence of boundary-free surfaces and beddings causes the superposition of incident and reflected sparse waves, which affects the vibration response of the far field. It is noteworthy that this superposition phenomenon was not clearly observed in the vibration response of the three-layer 5 cm-thick concrete slab.

Under the condition that the size of the layered medium is limited, when the total thickness of the layered medium is kept constant and the number of layers is varied, the greater the number of layers at the same impact energy and the greater the vibration velocity response will be. This is due to the complex transmission and reflection of waves at the interlayer interface and the boundary-free surface, resulting in an enhanced vibrational response at the surface of the finite-boundary layered medium.

5.2.2. Dimensional Analysis. For the multilayer medium without the cemented filling layer, the main factors affecting the vibration response under impact loading are as follows: drop-weight mass m, drop height H, gravity acceleration g, drop-weight density ρ_1, elastic modulus of the hammer E_1, thickness of the concrete slab h, density of the concrete slab ρ_2, elastic modulus of the concrete slab E_2, number of layers of the concrete slab n, and the distance from the measuring point to the impact point R.

Referring to Section 5.1.3, an expression for the impact vibration response of a multilayer concrete slab without a cementitious filler layer is given by

$$v\sqrt{\frac{\rho_1}{E_1}} = \phi\left(\frac{m}{\rho_1 R^3}, \frac{g\rho_1 R}{E_1}, \frac{H}{R}, \frac{h}{R}, n\right). \tag{13}$$

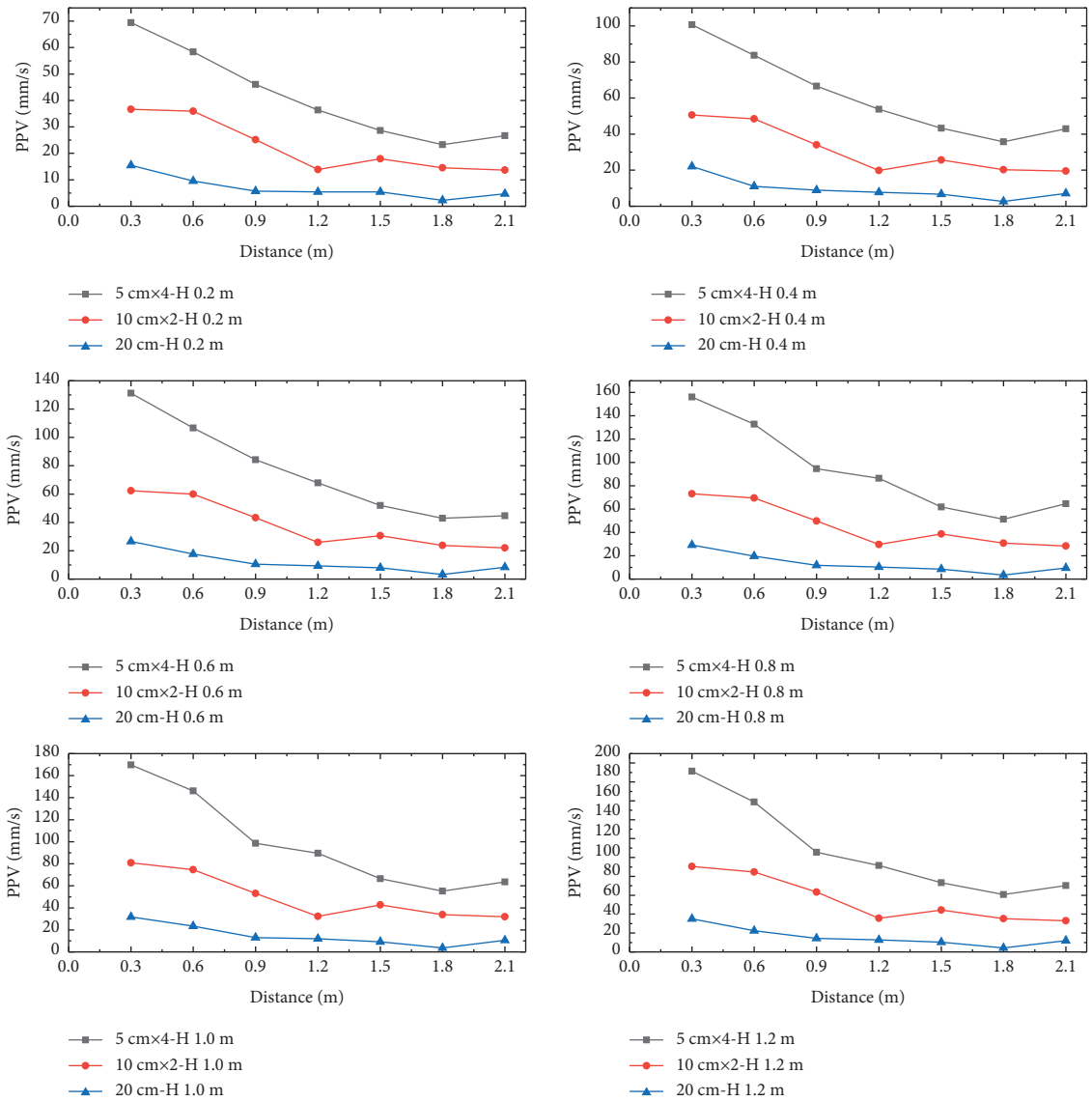

Figure 16: Peak vertical vibration velocity of multilayer concrete slabs without a cemented filling layer: 5 cm × 4 and 10 cm × 2 and 20 cm.

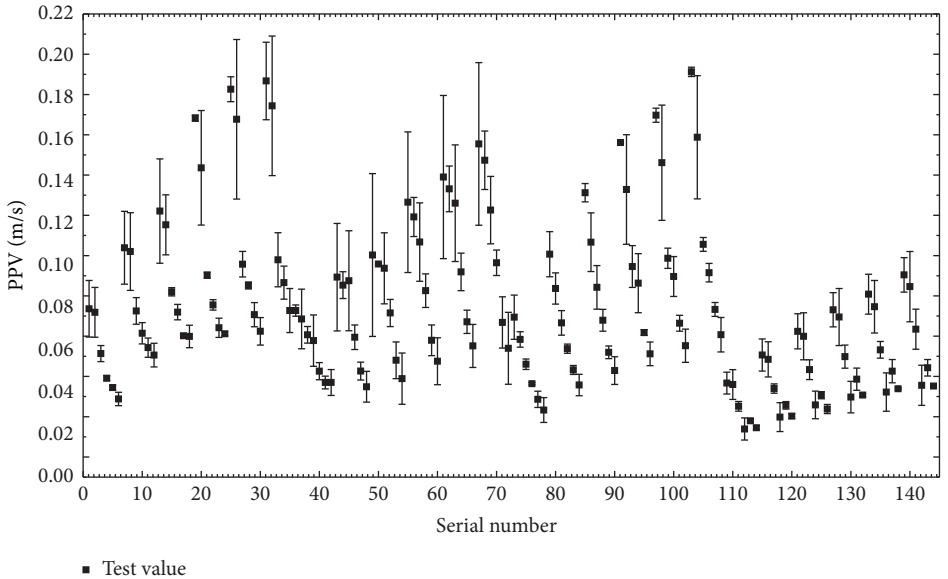

Figure 17: Error between the fitted and experimental values.

Figure 18: Layout of the cemented layer.

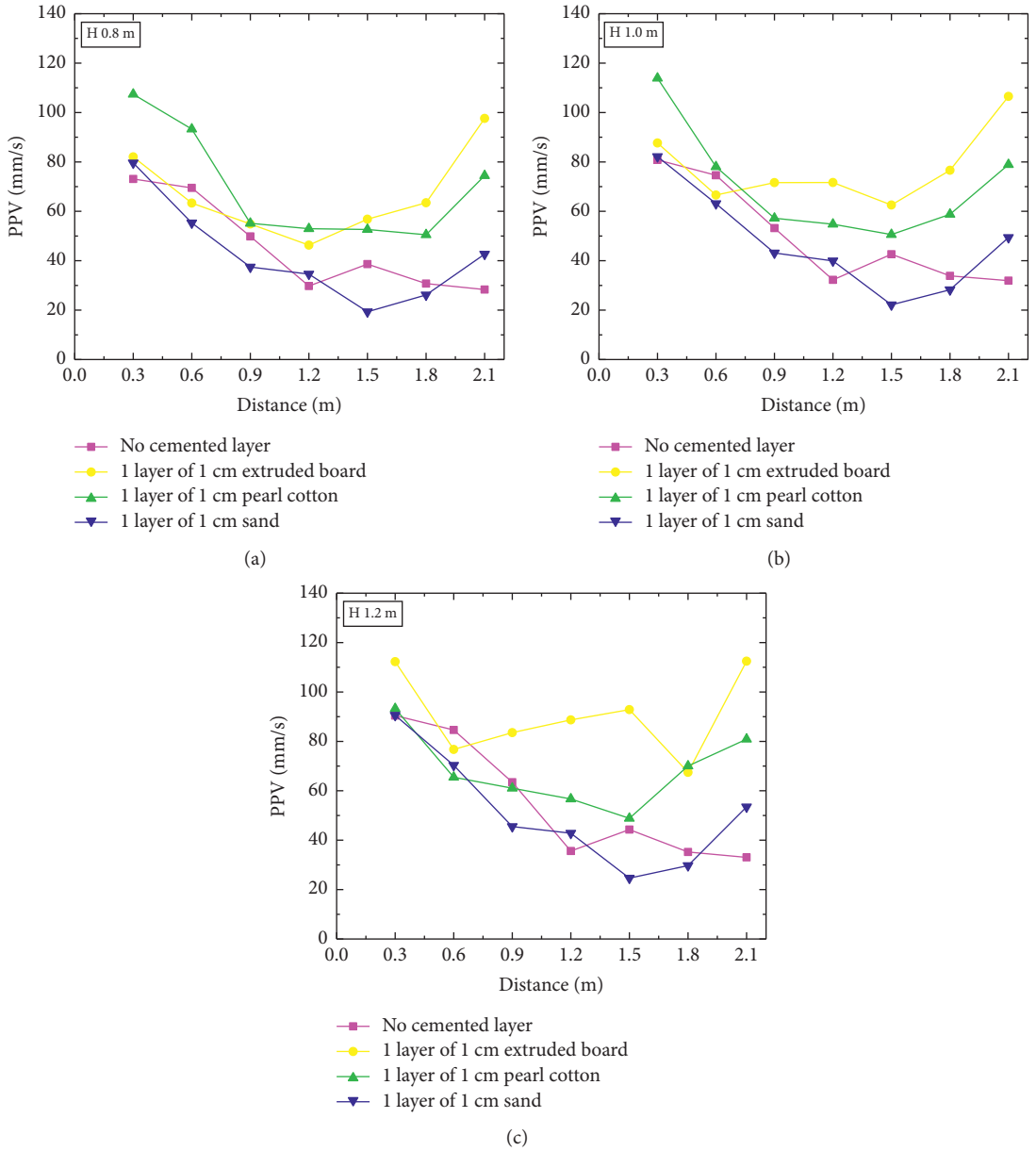

Figure 19: Peak vertical vibration velocity of a double-layer concrete slab containing a single 1 cm cemented layer of different materials: (a) H: 0.8 m; (b) H: 1.0 m; (c) H: 1.2 m.

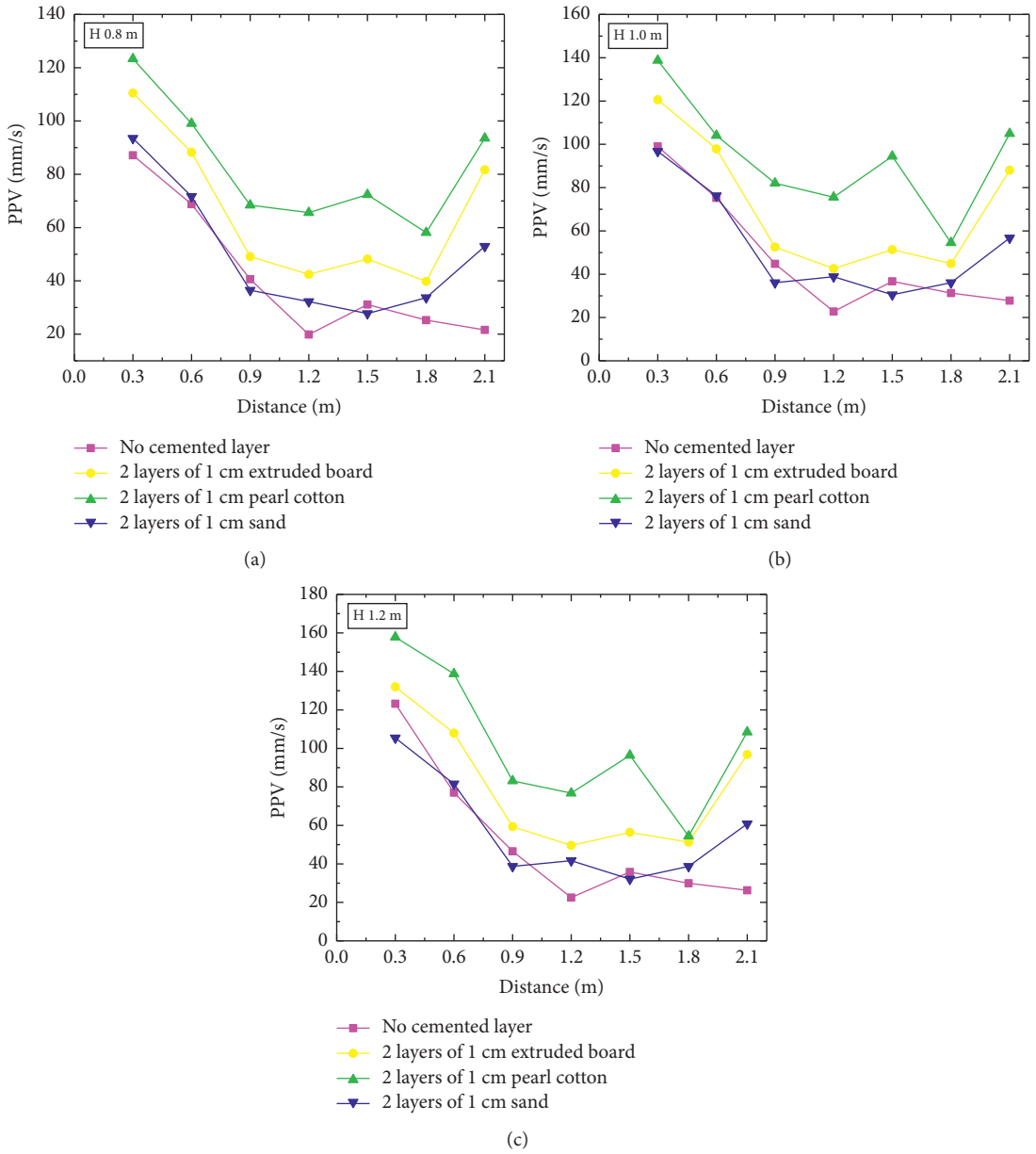

Figure 20: Peak vertical vibration velocity of a three-layer concrete slab containing double 1 cm cemented layers of different materials: (a) H: 0.8 m; (b) H: 1.0 m; (c) H: 1.2 m.

(1) Multiple linear regression is

$$v = 0.12 + 1.1316\frac{m}{\rho_1 R^3} - 125700\frac{g\rho_1 R}{E_1} + 0.0366\frac{H}{R} - 0.4792\frac{h}{R} - 0.00058528n. \quad (14)$$

Goodness of fit of the regression model is $R^2 = 0.8391$.

(2) Multiple power function regression is

$$v = \left(\frac{m}{\rho_1 R^3}\right)^{0.4248}\left(\frac{g\rho_1 R}{E_1}\right)^{0.1344}\left(\frac{H}{R}\right)^{0.4769}\left(\frac{h}{R}\right)^{-1.0571} n^{-0.1244}. \quad (15)$$

Goodness of fit of the regression model is $R^2 = 0.894536$.

By comparing the goodness of fit of the two sets of functions obtained by regression analysis, it is determined that the peak vertical vibration velocity function in the form of multivariate power function is more reasonable. Figure 17

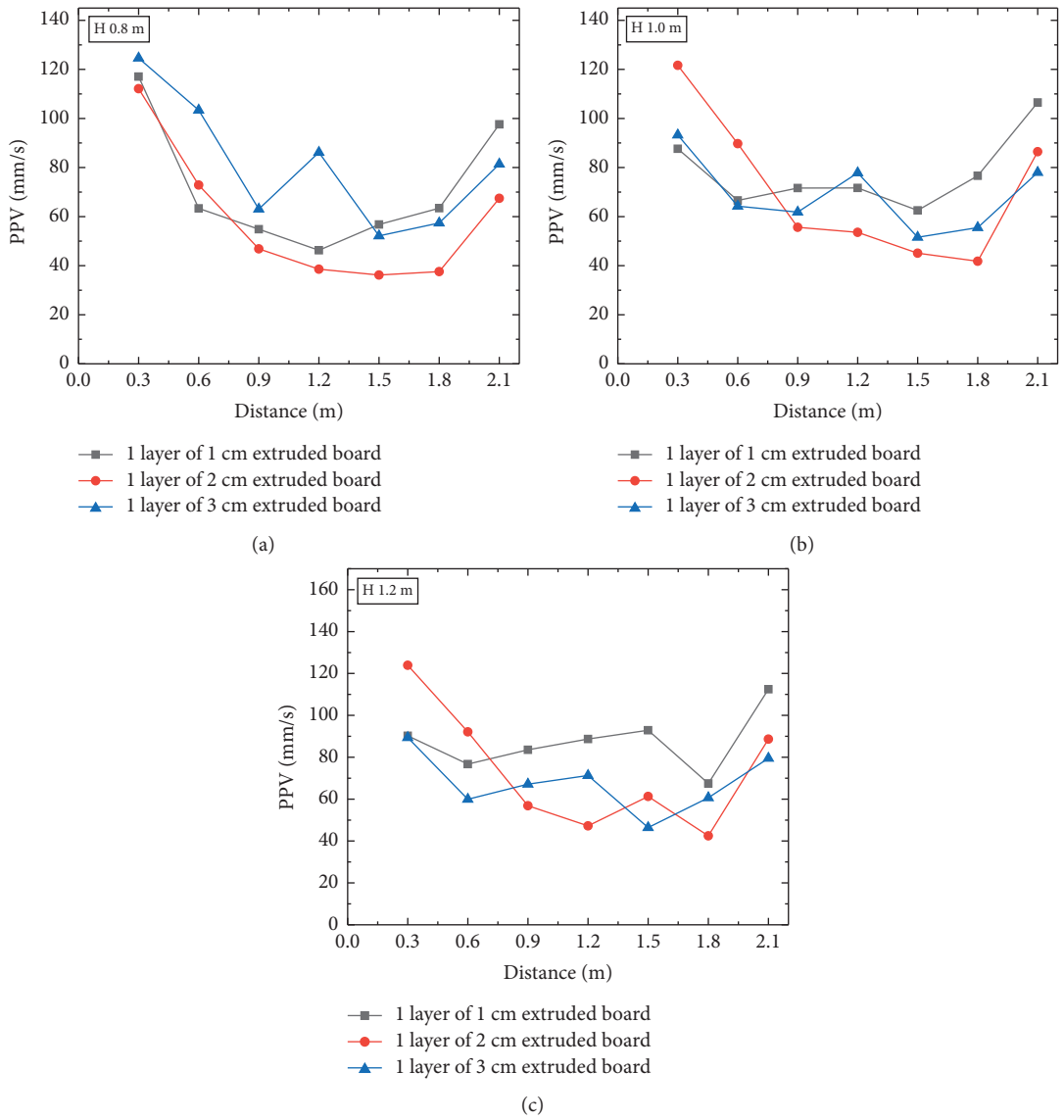

Figure 21: Peak vertical vibration velocity of a double-layer concrete slab containing a single layer of extruded plate of different thicknesses: (a) H: 0.8 m; (b) H: 1.0 m; (c) H: 1.2 m.

shows the error between the fitted and experimental values after the power function regression. The residual sum of squares after regression with the power function is RSS = 0.024413 and the root mean square error is RMSE = 0.01302.

5.3. Impact Loading Test Results and Discussion of Multilayer Concrete Slabs with Cemented Filling Layers. Three kinds of materials, EPE pearl cotton, XPS extruded board, and sand, were used as the cemented filling layer to investigate the effects of the cemented layer material and thickness on the vibration response of the layered medium. The thickness of the bonding layer is controlled to be ≤30% of the thickness of the single layer. The specific layout of the cemented layer in the test is shown in Figure 18. After the impact loading was completed using the simple drop hammer device, the test results are shown in Figures 19–22 .

As can be seen in Figures 19–22, the overall trend of fast decay in the near field and slow decay in the far field is maintained as the distance from the measuring point to the impact point increases. However, while maintaining the general trend, there are irregular fluctuations in the mass velocity response. In the far-field region, the increased vibration response still occurs to varying degrees at measuring points near the free surface. Compared to single-layer plates and multilayer plates without glued layers, for the first time, there is a forward shift in the position of the mass point caused by the superposition of stress waves leading to an increased vibration response.

From Figures 19 and 20, it is not so difficult to see that the change of the cemented layer material has a significant effect on the vibration response. The results of the vibration test with a 1 cm sand fill are closer to those without the colluvium. It can be deduced that this is due to the fact that of the three different cementing materials, the properties of

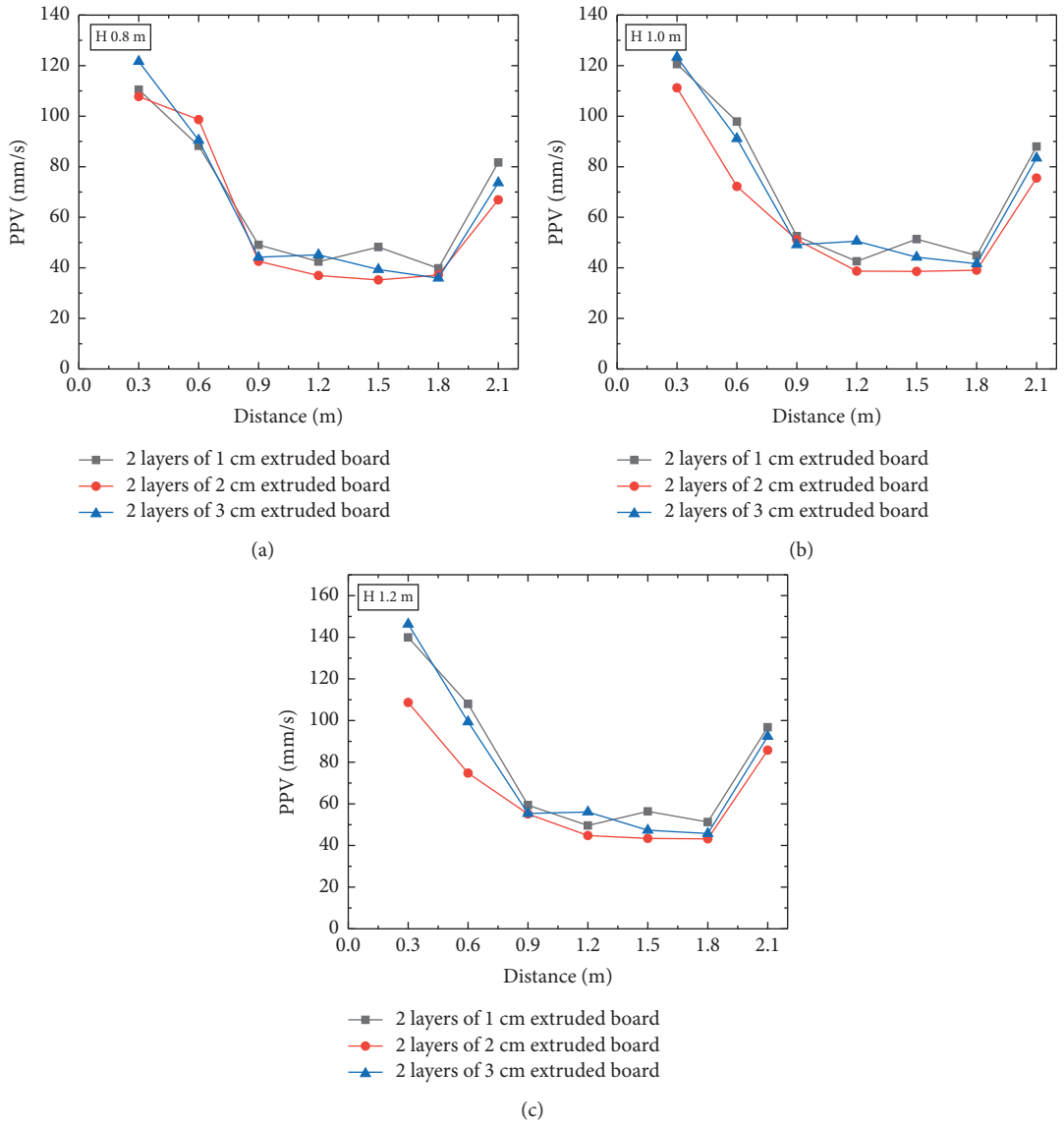

Figure 22: Peak vertical vibration velocity of a three-layer concrete slab containing two layers of extruded plates of different thicknesses: (a) H: 0.8 m; (b) H: 1.0 m; (c) H: 1.2 m.

the sandy soil are most similar to those of concrete. As the material properties of EPE pearl cotton and XPS extruded board differ significantly from those of concrete, the addition of both causes the test results to deviate significantly from those without the cemented layer. And, it is difficult to discern the significance of the effect on vibration response exhibited by these two materials. The test results for a two-layer concrete slab with a binder layer show that the XPS extruded board has a greater influence on the vibration response; however, in the case of a three-layer concrete slab with a binder layer, the EPE pearl cotton has a greater influence on the vibration response.

As shown in Figures 21 and 22, in the context of this experiment, the variation in the thickness of the cemented layer has some effect on the dynamic response in the context of this test, but the effect is small and irregular.

In summary, the filling of the cemented layer makes the vibration response of the layered concrete slab under impact loading more complex and exhibits a significant disorder. The lower the similarity between the material properties and dimensions of the layers, the higher the complexity of the overall dynamic characteristics of the layered media, that is, the more complex the overall vibration response of the layered media under impact loading.

6. Conclusions

In impact loading tests with concrete slabs (single, layered, and layered with cemented filler layers) as the working medium and self-developed simple falling hammer devices as the power source, the following conclusions were reached:

(1) Under the impact load, as the distance to the impact source increases, the vibration response of the surface of the dielectric layer gradually decreases due to energy diffusion and the damping effect of the material, showing a decay law of fast decay in the near field and slow decay in the far field, and the vibration energy moves towards the low-frequency components. As the impact energy increases, the vibration response on the surface of the media layer gradually increases and the difference in vibration response due to the impact energy gradually decreases with increasing distance. The vibration response of the dielectric layer surface and the thickness of the dielectric layer are negatively correlated, and the difference in vibration response due to impact energy decreases with the increase in the thickness of the dielectric layer.

(2) For finite-sized layered media, the presence of beddings and boundary-free surfaces causes a series of transmissive effects to occur during wave propagation. The results are as follows: (1) When the overall thickness of the layered medium remains constant and the number of layers increases, the vibration response of the layered medium surface enhances. (2) Near the free surface of the border away from the source, the velocity response increases as the distance to the source increases.

(3) The filling of the cemented layer makes the vibration response of the layered concrete slab under impact loading more complex and exhibits a significant disorder. The lower the similarity between the material properties and specifications of each layer of media, the higher the complexity of the overall dynamic characteristics of the layered medium, that is, the more complex the overall vibration response of the layered medium under impact loading.

(4) The relationship between the vibration response and the influencing factors was established by means of a dimensional analysis for impact loading of single-layer media and layered media without a cemented filling layer. By comparing the results of multiple regression analysis, the function expression with higher regression accuracy was selected from the two forms of multivariate linear function and multivariate power function to describe the vibration response under the impact load. It will hopefully provide an idea for determining the peak response of vibration velocity in the layered media.

Data Availability

The data used to support the findings of this study are available from the corresponding author upon request.

Conflicts of Interest

The authors declare no conflicts of interest in this article.

Acknowledgments

This work was supported by the National Natural Science Foundation of China (No. 51874118), the Fundamental Research Funds for the Central Universities (No. 2018B667X14), and Postgraduate Research and Practice Innovation Program of Jiangsu Province, China (No. KYCX18_0567).

References

[1] W. T. Thomson, "Transmission of elastic waves through a stratified solid medium," *Journal of Applied Physics*, vol. 21, no. 2, pp. 89–93, 1950.

[2] N. A. Haskell, "The dispersion of surface waves on multilayered media," *Bulletin of the Seismological Society of America*, vol. 43, no. 1, pp. 17–34, 1953.

[3] N. A. Haskell, "Radiation pattern of surface waves from point sources in a multi-layered medium," *Bulletin of the Seismological Society of America*, vol. 54, no. 1, pp. 377–393, 1964.

[4] E. Pestel and F. A. Leckie, *Matrix Methods in Elastomechanics*, Vol. 435, McGraw-Hill, New York, NY, USA, 1963.

[5] L. Knopoff, "A matrix method for elastic wave problems," *Bulletin of the Seismological Society of America*, vol. 54, no. 1, pp. 431–438, 1964.

[6] E. N. Thrower, "The computation of the dispersion of elastic waves in layered media," *Journal of Sound and Vibration*, vol. 2, no. 3, pp. 210–226, 1965.

[7] J. W. Dunkin, "Computation of modal solutions in layered, elastic media at high frequencies," *Bulletin of the Seismological Society of America*, vol. 55, no. 2, pp. 335–358, 1965.

[8] T. H. Watson, "A note on fast computation of Rayleigh wave dispersion in the multilayered elastic half-space," *Bulletin of the Seismological Society of America*, vol. 60, no. 1, pp. 161–166, 1970.

[9] P. W. Buchen and R. Ben-Hador, "Free-mode surface-wave computations," *Geophysical Journal International*, vol. 124, no. 3, pp. 869–887, 1996.

[10] C. H. Chapman, "Yet another elastic plane-wave, layer-matrix algorithm," *Geophysical Journal International*, vol. 154, no. 1, pp. 212–223, 2003.

[11] D. Pei, J. N. Louie, and S. K. Pullammanappallil, "Improvements on computation of phase velocities of Rayleigh waves based on the generalized R/T coefficient method," *Bulletin of the Seismological Society of America*, vol. 98, no. 1, pp. 280–287, 2008.

[12] T. Liu, "Efficient reformulation of the thomson-haskell method for computation of surface waves in layered half-space," *Bulletin of the Seismological Society of America*, vol. 100, no. 5A, pp. 2310–2316, 2010.

[13] J. Lysmer, "Lumped mass method for Rayleigh waves," *Bulletin of the Seismological Society of America*, vol. 60, no. 1, pp. 89–104, 1970.

[14] G. Waas, "Linear two-dimensional analysis of soil dynamics problems in semi-infinite layer media," Ph. D. Thesis, University of California, Los Angeles, CA, USA, 1972.

[15] H. Tajimi, "Contribution to theoretical prediction of dynamic stiffness of surface foundations," *Proceedings of 7th World Conference on Earthquake Engineering*, vol. 5, pp. 105–112, 1980.

[16] G. Waas, H. R. Riggs, and H. Werkle, "Displacement solutions for dynamic loads in transversely-isotropic stratified media," *Earthquake Engineering & Structural Dynamics*, vol. 13, no. 2, pp. 173–193, 1985.

[17] E. Kausel, *An Explicit Solution for the Green Functions for Dynamic Loads in Layered media*, Department of Civil Engineering, School of Engineering, Massachusetts Institute of Technology, Cambridge, MA, USA, 1981.
[18] E. Kausel, "Thin-layer method: f," *International Journal for Numerical Methods in Engineering*, vol. 37, no. 6, pp. 927–941, 1994.
[19] R. Sen, "Green's function implementation for pile analysis," *Journal of Engineering Mechanics*, vol. 113, no. 4, pp. 594–609, 1987.
[20] S. Bougacha and J. L. Tassoulas, "Seismic analysis of gravity dams. I: modeling of sediments," *Journal of Engineering Mechanics*, vol. 117, no. 8, pp. 1826–1837, 1991.
[21] S. Bougacha, J. L. Tassoulas, and J. M. Roësset, "Analysis of foundations on fluid–f," *Journal of Engineering Mechanics*, vol. 119, no. 8, pp. 1632–1648, 1993.
[22] T. Nogami and M. Kazama, "Dynamic response analysis of submerged soil by thin layer element method," *Soil Dynamics and Earthquake Engineering*, vol. 11, no. 1, pp. 17–26, 1992.
[23] T. Nogami and M. Kazama, "Thin layer element method for dynamic soil-structure interaction analysis of axi-symmetric structure in submerged soil," *Soil Dynamics and Earthquake Engineering*, vol. 16, no. 5, pp. 337–351, 1997.
[24] L. Sun, Y. Pan, and W. Gu, "High-order thin layer method for viscoelastic wave propagation in stratified media," *Computer Methods in Applied Mechanics and Engineering*, vol. 257, pp. 65–76, 2013.
[25] J. Yang, Y. Li, H. Xie, Z. Song, and L. Tian, "Stress wave propagation and energy dissipation in jointed rocks," *Chinese Journal of Rock Mechanics and Engineering*, vol. 25, no. 12, pp. 2426–2434, 2006.
[26] Q. Z. Wang, S. Zhang, and H. P. Xie, "Rock dynamic fracture toughness tested with holed-cracked flattened Brazilian discs diametrically impacted by SHPB and its size effect," *Experimental Mechanics*, vol. 50, no. 7, pp. 877–885, 2010.
[27] F. Lu, Y. Lin, X. Wang, L. Lu, and R. Chen, "A theoretical analysis about the influence of interfacial friction in SHPB tests," *International Journal of Impact Engineering*, vol. 79, pp. 95–101, 2015.
[28] J. C. Li, N. N. Li, H. B. Li, and J. Zhao, "An SHPB test study on wave propagation across rock masses with different contact area ratios of joint," *International Journal of Impact Engineering*, vol. 105, no. 105, pp. 109–116, 2017.
[29] Y. Yang, R. S. Yang, and J. G. Wang, "Simulation material experiment on dynamic mechanical properties of jointed rock affected by joint thickness," *Journal of China University of Mining & Technology*, vol. 45, no. 2, pp. 211–216, 2016.
[30] W. Wang, K. Li, Z. Yan, and X. Tang, "Study on the closure deformation properties of joint fractal under SHPB load," *Gold Science and Technology*, vol. 25, no. 1, pp. 75–83, 2017.
[31] G. Challita and R. Othman, "Finite-element analysis of SHPB tests on double-lap adhesive joints," *International Journal of Adhesion and Adhesives*, vol. 30, no. 4, pp. 236–244, 2010.
[32] Z. Tian, S. Li, and N. Xiao, "Experimental studies and numerical simulation of stress wave propagation in one-dimensional rock mass," *Chinese Journal of Rock Mechanics and Engineering*, vol. 27, no. S1, pp. 2687–2693, 2008.
[33] B. Sun, S. S. Guo, S. Zeng, A. Y. Ma, and X. S. Deng, "Transmission and reflection and the attenuation law of stress wave in layered joint rock mass," *Journal of disaster prevention & mitigation engineering*, vol. 35, no. 6, pp. 828–832, 2015.
[34] S. Li and J. Cheng, "Experimental study on characteristics of stress wave propagation in mesoscale and complex rock mass by microseismic monitoring," *Chinese Journal of Geotechnical Engineering*, vol. 36, no. 2, pp. 312–319, 2014.
[35] Z. J. Wang, X. L. Li, L. Ge, and P. Y. Wang, "Free-field stress wave propagation induced by underground chemical explosion in granite," *Chinese Journal of Rock Mechanics and Engineering*, vol. 11, pp. 1827–1831, 2003.
[36] E. Buckingham, "On physically similar systems; illustrations of the use of dimensional equations," *Physical Review*, vol. 4, no. 4, pp. 345–376, 1914.